IEEE Photonics Journal
An IEEE Photonics Society Publication

Open Access

Optimization of Dual-Channel Near-Infrared Non-Invasive Glucose Level Measurement Sensors Based On Monte-Carlo Simulations

Volume 13, Number 3, June 2021

Murad Althobaiti
Ibraheem Al-Naib

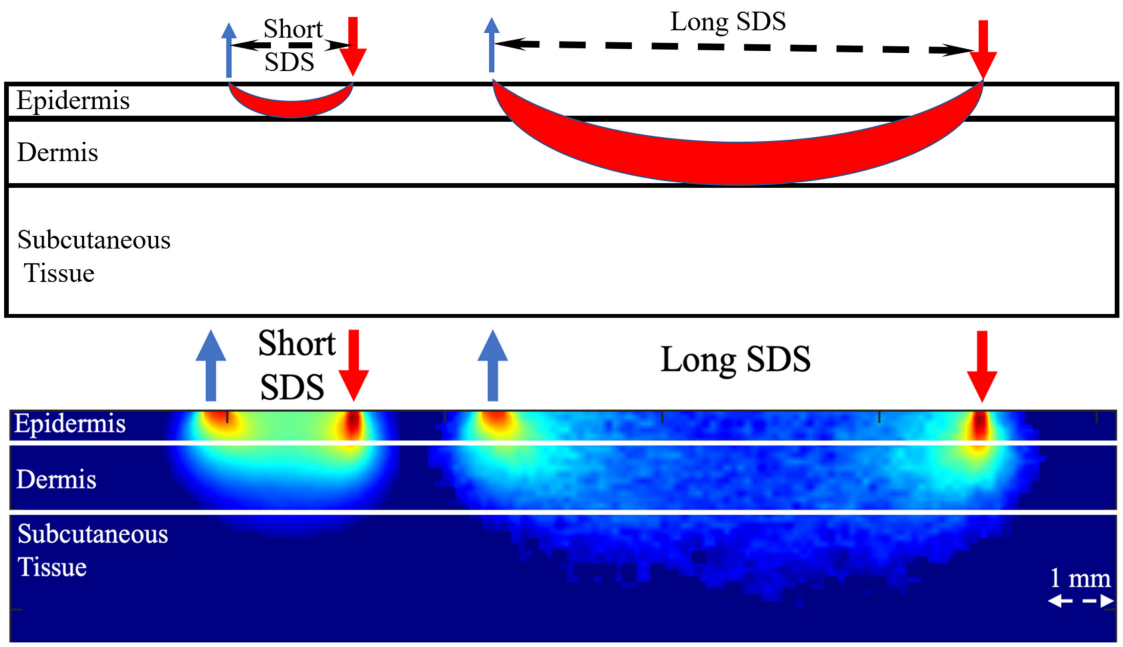

DOI: 10.1109/JPHOT.2021.3079408

IEEE photonics SOCIETY

IEEE

Optimization of Dual-Channel Near-Infrared Non-Invasive Glucose Level Measurement Sensors Based On Monte-Carlo Simulations

Murad Althobaiti and Ibraheem Al-Naib

Biomedical Engineering Department, College of Engineering, Imam Abdulrahman Bin Faisal University, Dammam 31441, Saudi Arabia

DOI:10.1109/JPHOT.2021.3079408

Manuscript received April 1, 2021; revised May 5, 2021; accepted May 9, 2021. Date of publication May 14, 2021; date of current version May 28, 2021. This work was supported by Deputyship for Research & Innovation, Ministry of Education in Saudi Arabia through the Project IF-2020-013-Eng at Imam Abdulrahman bin Faisal University/College of Engineering. Corresponding author: Ibraheem Al-Naib (e-mail: iaalnaib@iau.edu.sa).

Abstract: Non-invasive glucose monitoring sensors are promising techniques in diabetes management. In particular, optical-based near-infrared glucose sensors are label-free, compact, user-friendly, and inexpensive. They require no daily calibration and can provide continuous glucose level monitoring. However, these sensors are still in the development stage since their accuracy is still not widely accepted by medical professionals. Here, we introduce an optimized dual-channel approach for this kind of sensor where four optodes for short and long channels are employed. The long channel signal that contains useful information about the glucose level can be utilized to calculate the glucose contents in the dermis layer of the skin while the short channel is utilized to measure the interference "noise" signal originating from the epidermis layer. So, the latter can then be removed from the long channel signal. This work investigates the optimal source-detector separation (SDS) of both short and long channels for a wide range of wavelengths from 1200 nm to 1900 nm. Based on the sensitivity distributions of both dermis and epidermis layers and the signal-to-noise ratio, it is suggested that a 2 mm SDS distance with a wavelength of 1450 nm is a potential choice for the short channel. Moreover, 6 mm SDS at the wavelength of 1750 nm is the optimal choice for the long channel. This work may pave the way for further optimization of non-invasive near-infrared glucose sensors that will be widely adopted in the healthcare sector.

Index Terms: Near-infrared, glucose sensors, Monte-Carlo simulations.

1. Introduction

The Demand for low-cost and compact biosensors for diabetes management is increasingly growing [1]–[6]. Currently existed glucose monitors employ advanced electrochemical reaction techniques to estimate glucose levels in the blood [7]. However, electrochemical sensors have a limited lifetime, low accuracy and they are not user-friendly sensors [8], [9]. Alternatively, optical-based glucose measurement techniques have the advantages to overcome many limitations of electrochemical sensors and have been of particular emphasis in the advancement of non-invasive glucose sensors so far [10]–[14]. Continuous glucose monitoring sensors (CGMS) are currently available in the markets [15], [16]. These sensors provide measurements of the glucose levels

every 1–5 minutes. It consists of a small filament that is inserted beneath the skin and glucose is measured based on an enzymatic reaction. However, due to the immune response of the body and degradation of reagents, these sensors have to be regularly replaced [17]. Additionally, the daily calibration needed for the CGMS and the short lifetimes for these devices is a clear disadvantage for the end-users as they are expected to be used for long-term periods. Noninvasive glucose monitoring sensors are now considered as potential alternatives to address the difficulties with the current CGMS [10], [18], or at least a potential complement of the CGMS. These types of sensors are still in the development stages and few are commercially available based on reverse iontophoresis and impedance spectroscopy [19]–[21]. These two sensors faced clinical challenges since the GlucoWatch lead to skin irritation. Additionally, the accuracy was found to be less than what it was in the stages of the clinical trials. Due to its low accuracy, user discomfort, and high cost, the sensors were shortly stopped after their release [22], [23].

In the near-infrared (NIR) spectroscopy field, many techniques were extensively investigated to noninvasively measure the glucose level in the blood. Short wavelengths band of the NIR spectrum was evaluated for finger spectra measurements [24], [25]. Interestingly, the authors of Ref. [26] investigated the correlation between dermal interstitial fluid glucose and plasma glucose. According to this pioneering study, there is no significant difference between measuring glucose levels from dermal glucose and plasma glucose. The epidermis has the stratum corneum which consists of dead cells. Therefore, the epidermis acts as a shield and of the important signal that originates from the dermis layer. In turn, it degrades the total signal received by the detector by adding an interference noise to any measured signal. Hence, it does not contribute to any useful information about blood glucose levels [27]. Later on, a NIR system was proposed by Maruo *et al.* to detect quite low glucose level signals from human dermis tissue [28]. This is because the capillaries are well developed in the dermis layer. The authors tried also choosing an optimal source-detector separation (SDS) to detect the signal from the dermis layer, but they did not exclude the interference noise coming from the epidermis layer. Hence, the artificial noise coming from the epidermis layer can be, in principle, removed if we can selectively measure both signals, i.e., from the dermis and the epidermis layers at the same time.

In the field of functional near-infrared spectroscopy (fNIRS) neuroimaging, a similar challenge faced the scientific community [29]–[31]. In this regard, the researchers are interested in measuring hemodynamic brain activities. However, the fNIRS backscattered light not only carries brain activities measurements but also measurements from superficial layers such as the skin. In order to get a full picture of activities changes in brain tissue, one needs to eliminate the influence of these superficial signals. To overcome this challenge and to selectively eliminate these sources of interference, one would need to conduct additional measurements that are exclusively picking up the signals from these superficial layers, and then correct the deeper measurements accordingly [30], [32]. The depth of light propagation is dependent on the separation between the light-receiving and the light-transmitting optodes. When the SDS is short, the light interacts with the superficial layers and the channels are called short-separation channels. Vice-versa, when the light interacts with deep layers, the channels are called long-separation channels. Utilizing the short SDS channels, various superficial noise removal methods have been developed [30], [33]–[35]. More specifically, a general linear model with principal component analysis has been successfully utilized to remove the short-separation channel component from the regular long-separation fNIRS channels [36].

Recently, different optical-based near-infrared approaches to improve the measurement accuracy of glucose level in the blood have been reported [37]–[39]. For instance, in order to eliminate the spectral variations from background interferences, a differential correction method utilizing a floating-reference position has been proposed [37]. This led to the weakening of the influence of background variations on the NIR spectroscopy. Moreover, a reflectance setup has been proposed with variable SDS to enable scattering-independent absorption measurement in order to enhance glucose concentration monitoring [38]. The approach was then evaluated using Monte Carlo (MC) simulations. A similar setup was also proposed to enable an effective separation of diffusion and absorption signals [39]. The authors of that paper employed MC simulations and acquired the

optimal SDSs at the 1000∼1600 nm range. This approach helped to boost the glucose sensitivity in the two acquired signals.

In this study, we aim to investigate optimal SDS for short and long channels for non-invasive glucose level measurement sensors. In choosing the optimal SDS for the short channel for signal measurements from the epidermis layer, two important factors need to be considered. First, as the SDS decreases, it means low penetration depths, which also means minimum dermis sensitivity. Vice versa, when the SDS increases, a contribution from the dermis layer into the signal will reduce the efficiency of the measurements. Secondly, in case the SDS decreases to a very small value, we may have a design limitation to build a reliable prototype because of the optical fiber size. Therefore, it is preferred from the design point of view to have a practical SDS to build a reliable prototype. Therefore, we need to find an optimal SDS for the short channel in which you increase the SDS but not significantly increases the dermis sensitivity. Similarly, in choosing the optimal SDS for long channel separation for dermis measurements, high dermis sensitivity is achieved by increasing the SDS. However, signal-to-noise (SNR) will decrease when the separation is very large. Therefore, a balance between high dermis sensitivity and acceptable SNR should be carefully considered. In addition to the above-discussed factors, choosing an optimal SDS also depends on the wavelength. Thus, choosing the right wavelength is essential to reach an optimum configuration of the sensors. The rest of the paper is organized as in the following: Section 2 introduces the methodology used in this paper. Next, Section 3 present the results and its discussion, and the paper is summarized in Section 4.

2. Methodology

To study the above hypothesis, Monte Carlo Simulation (MCS) has been used to simulate the propagation of light in skin tissue for a wide range of wavelengths from 1200 nm to 1900 nm. This simulation approach is adequate and widely used by scientists for strongly scattering media such as skin tissues [40], [41]. In MCS, the transport of each photon in the tissue layers is modeled based on the probability distribution of the events, i.e., absorption and scattering. In the actual computation, the light flux is split into millions of photons, and each photon propagation history is traced with pre-knowledge of the optical properties of the tissue. The optical properties that are considered in this simulation are the absorption coefficient (μ_a), scattering coefficient (μ_s), and refractive index (n) that are all wavelength dependent. The optical properties for the range of interest used in this simulation are taken from Ref. [28] that were determined based on Refs. [42], [43]. These properties reflect the constitutes of these layers including glucose, which has many absorption lines including some strong absorption peaks outside the studied range. From a practical point of view, especially when using compact photodiodes with low output power, it is rather not desirable to choose a wavelength with very strong absorption as that will lead to an extremely small signal at the detector position.

Fig. 1 presents an illustration diagram of the light propagation paths via skin tissue. The skin contains three layers: epidermis with a thickness of 0.3 mm which is the outermost layer of skin, dermis with a thickness of 1 mm, and the deeper subcutaneous tissue layer. The size of the considered model in this paper is a $16 \times 16 \times 16$ mm^3 cubic volume with a voxel size of 0.1 mm. The light sources and the detectors were simulated as pencil sources and disk detectors. For each simulation run, a fluence distribution was acquired for each source and detector channel. An ideal short SDS channel should have no sensitivity to the dermis and an ideal long SDS channel should exhibit the highest sensitivity distribution from dermis tissue.

Obtaining this ideal short SDS channel scenario is impractical because the defined geometry and the sensitivity distributions are continuous functions. Practically, the aim is to minimize dermis sensitivity (DS) at a reasonable SNR for optimal short channel separation and maximize DS for optimal long channel separation. Thus, we considered three metrics in order to categorize the performance of the system at a wide range of wavelengths and for a sweep of SDSs. For each model, we computed the DS which describes how sensitive a particular channel is to the dermis layer contents comparative to the overall sensitivity. It is the voxel-wise sum of the photon

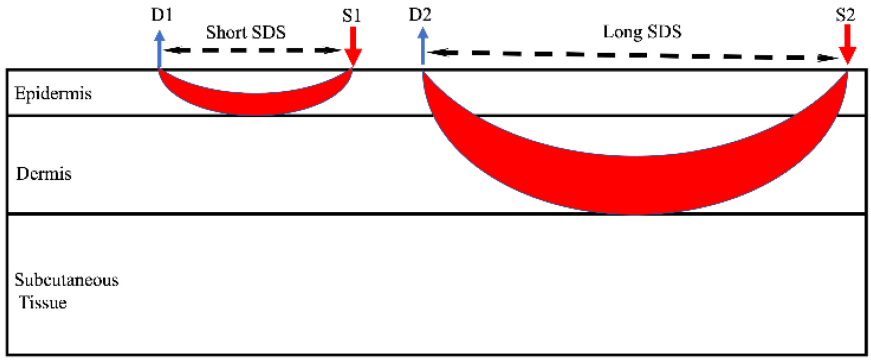

Fig. 1. Schematic of the blood glucose monitoring (dual channels) near-infrared sensor. Two sources and two detectors are placed at different source-detector separations (SDS).

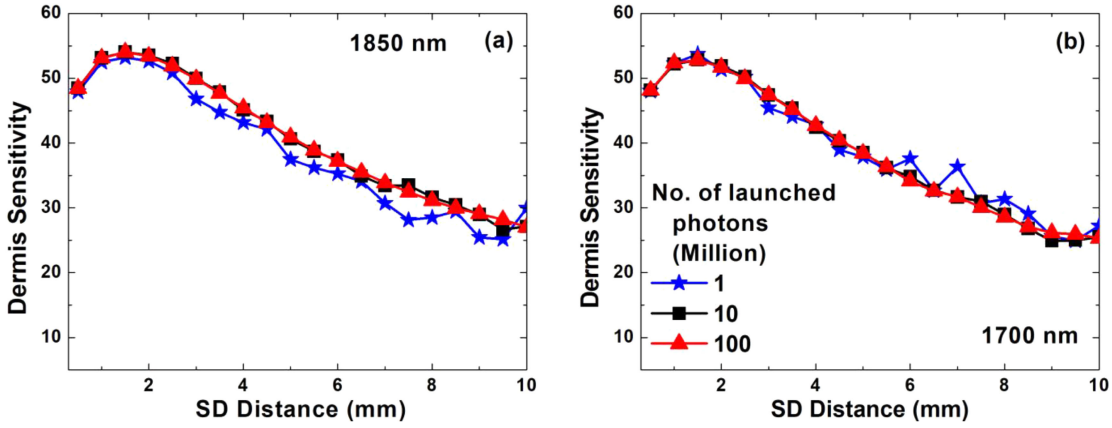

Fig. 2. Dermis sensitivity versus SDS for (a) 1850 nm and (b) 1700 nm with sweep values of the number of launched photons ranging from 1 to 100 million photons.

measurement density function (PMDF) in the dermis layer divided by the voxel-wise sum of the whole PMDF for each model is given by:

$$DS = 100 \times \frac{\sum_{Dermis} PMDF}{\sum_{total,} PMDF} \tag{1}$$

In order to choose enough number of simulated photons for the given system, we evaluated the dermis sensitivity for two wavelengths, namely 1850 and 1700 nm, versus the SDS for 1 Million (M), 10 M, and 100 M photons that launched at the beginning of the experiment. As the number of photons is increased, the sensitivity value should basically converge. Fig. 2 presents the results where it is observed that indeed using 100 M gives almost the same value as using 10 M. Moreover, reaching a convergence at small separation can take place even with 10 M, while the 100 M is required for the long separation which seems to be logical.

Likewise, we also have computed the epidermis sensitivity (ES) which gives how sensitive a particular channel is to the epidermis layer contents comparative to its overall sensitivity is given by:

$$ES = 100 \times \frac{\sum_{Epidermis} PMDF}{\sum_{total,} PMDF} \tag{2}$$

As the depth of the epidermis is shallower than the dermis, we expect the convergence to take place with a smaller number of photons for the epidermis sensitivity compared to the dermis

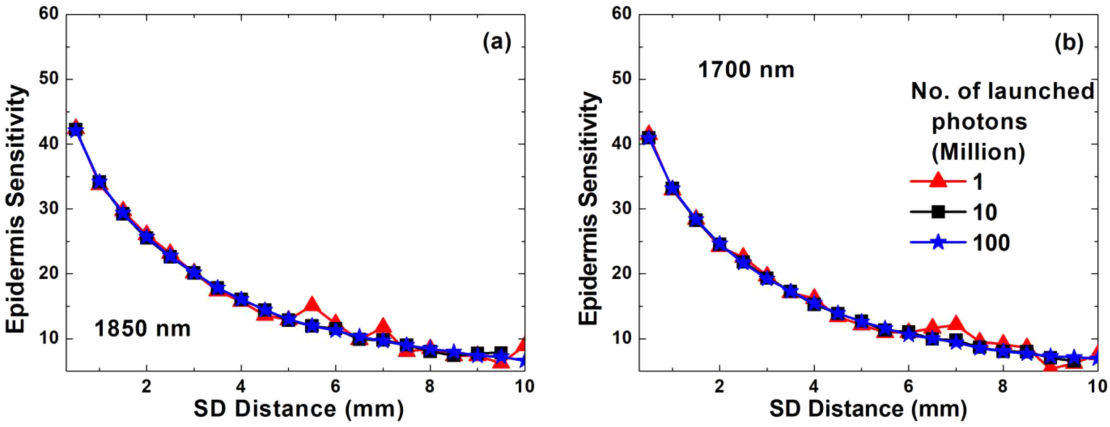

Fig. 3. Epidermis sensitivity versus SDS for (a) 1850 nm and (b) 1700 nm with a sweep of values of the number of launched photons ranging from 1 to 100 million photons.

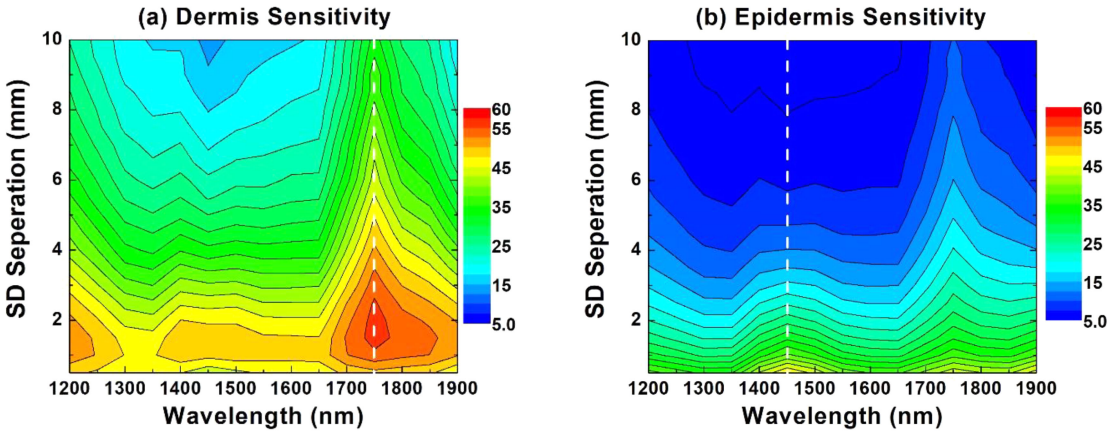

Fig. 4. (a) Dermis and (b) epidermis sensitivity distribution for source-detector separations between 0.5 mm to 10 mm with a step size of 0.5 mm. The figure shows a sensitivity portfolio for a range of wavelengths between 1200 nm and 1900 nm.

sensitivity. Nevertheless, we have evaluated the epidermis sensitivity with the same range of launched photons as shown in Fig. 3. Indeed, the convergence seems to take place even when the number of photons is just 10 M.

We also computed the SNR for each SDS to evaluate the response at each wavelength when the SDS increases from 0.5 mm to 10 mm with a step of 0.5 mm. According to Ref. [44], the SNR can be computed by running multiple (here we used N = 15 and N = 30) independently seeded MC simulations to obtain the mean, μ, and standard deviation, σ, at any particular voxel in the model, then converting that to dB as given by Eq. (3).

$$SNR\,(SD) \;=\; 20\log_{10}\frac{\mu\,(SD)}{\sigma\,(SD)} \tag{3}$$

3. Results and Discussion

Fig. 4 shows dermis and epidermis sensitivities when sweeping the SD separations between the sources and the detectors and increasing the source wavelength from 1200 nm to 1900 nm with a step of 50 nm. For all wavelengths, increasing SD separations decreases the sensitivity. The goal here is to find suitable wavelengths for the short and long channels as explained in Fig. 1. Hence,

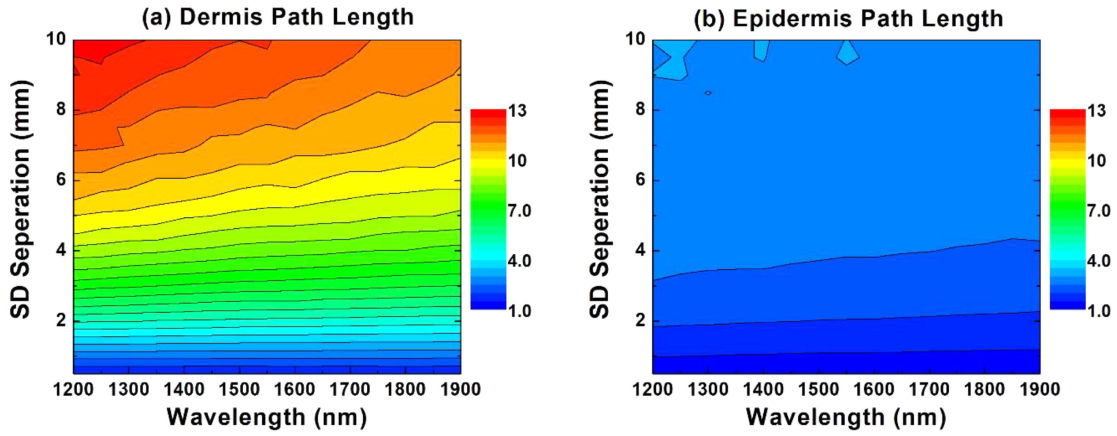

Fig. 5. (a) Dermis and (b) epidermis average path lengths in mm for source-detector separations between 0.5 mm to 10 mm with a step size of 0.5 mm.

the wavelength(s) with maximum sensitivity in the dermis layer for most or all separation distances will be a suitable candidate for the long channel provided that the separation is longer than the short channel. Observing Fig. 4(a), an optical wavelength of 1750 nm indicated by the white dashed line features the highest dermis sensitivity for the whole range of the SD separation. Hence, it is a good choice for the long channel. For the short channel, the wavelength with minimum sensitivity in the dermis layer and maximum sensitivity in the epidermis layer would be an optimal choice. According to the dermis sensitivity in Fig. 4(a), a wavelength between 1300 nm and 1650 nm is a good choice. Within this range, the epidermis sensitivity peaks at 1450 nm at 0.5 mm and decreases rapidly beyond SDS equals 3 mm. Therefore, a wavelength for the short channel should be chosen from this range with an SD separation smaller than 3 mm.

Next, Fig. 5 shows the average photon path length in the dermis and epidermis layers as a function of the SD separation. For the dermis layer, there is almost no change in the average path length for all wavelengths when the SD is less than 4 mm. Beyond that, there is a tendency for a larger average path length for the short wavelengths compared to the long wavelengths. In the epidermis layer, there are no significant changes in the average photon path lengths regardless of the wavelengths. It is worth mentioning that the average path length is heavily dependent on the concerned layer as well as the exact absorption and scattering coefficients that are wavelength-dependent. The results in Fig. 5(a) show that the average path length is long enough to interact with the glucose contents in the dermis layer. Also, there is no significant change in the path length for a small change in the light wavelength. Moreover, the average path length is shown in Fig. 5(b) for the epidermis layer is about 4 mm or less. The latter can be considered as the upper limit for the short channel in order to probe the contents of the epidermis layer.

Fig. 6 shows the calculated SNR for different SD separations. SNR can be calculated by running multiple (here we used $N = 15$ and $N = 30$) independently seeded MC simulations. To show the effect of calculating SNR with the number (N) of independently seeded MC simulations, we present in this figure the results of calculating SNR for nominal values of the wavelength 1750 nm and 1450 nm that were preliminary selected based on the sensitivity results shown in Fig. 4 for both $N = 15$ and $N = 30$ as well as ± 50 nm with reference to the 1750 nm and 1450 nm. The general trend for all wavelengths and a different number of independently seeded MC simulations is that the SNR decreases with increasing the SD separation. However, increasing the independently seeded MC simulations smoothed the curves as witnessed in Fig. 6. For the wavelength of 1400 nm, the average of the variations between $N = 15$ and $N = 30$ in the SNR was less than 5% and it is reduced to 2% when N was increased to 40. Therefore, we concluded that the $N = 30$ is sufficient. An SNR of 20 dB has been chosen as an acceptable threshold here and this value is detector sensitivity dependent. The designer can perhaps choose a lower value for the SNR if detectors

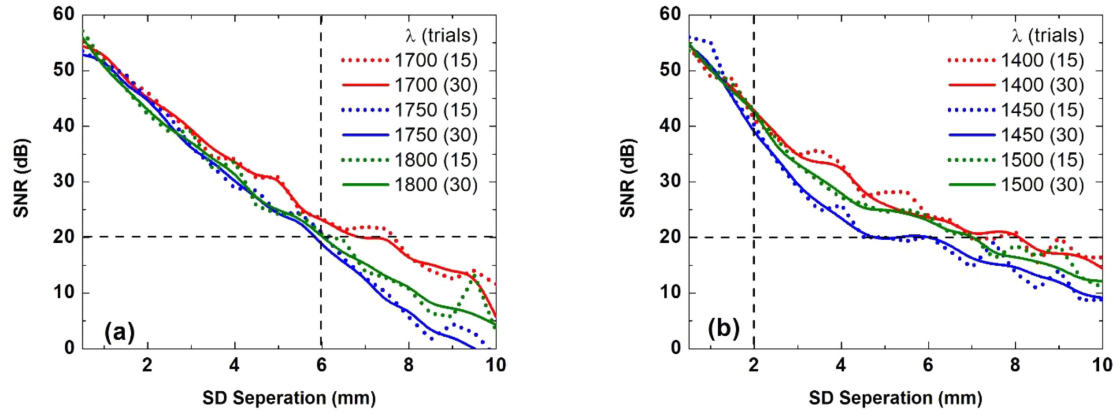

Fig. 6. Calculated SNR for SD separation between 0.5 mm and 10 mm for (a) long channel for wavelengths of 1700, 1750, and 1800 nm and (b) short channel for wavelengths of 1400, 1450, and 1500 nm, and for 15 and 30 different number of independently seeded MC simulations, respectively.

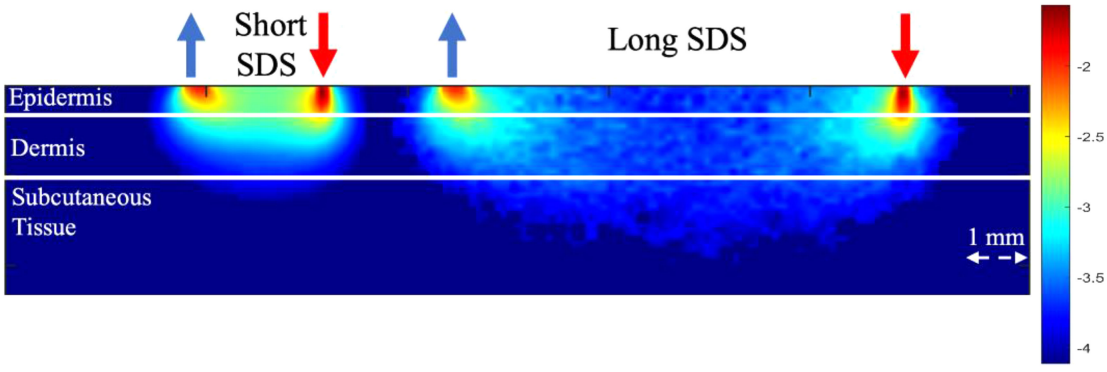

Fig. 7. Spatial sensitivity profile of photons (shown in $\log_{10}$ scale) in the skin as given by MC simulations for the dual-channel near-infrared sensor. In this example, the SDS for the short channel (left side) is 2 mm at 1450 nm and the SDS for the long channel (right-side) is 6 mm at 1750 nm.

with very high sensitivity are available. Fig. 6(a) shows that while the SNR is almost the same for all wavelengths for all SDS less than 3 mm, a divergence in the SNR emerge for a separation of 3 mm and beyond. More importantly, the SNR for the long channel drops below 20 dB for 6 mm SDS for all the wavelengths of 1700, 1750, and 1800 nm. Considering the sensitivity results in Fig. 4(a) and the SNR in Fig. 6(a) for these wavelengths for the long channel, it is evident that for the 1750 nm, the maximum allowed separation of 6 mm. This choice is based on the fact that the sensitivity drops from 43.7 at 1750 nm to 34.1 only at 1700 nm and there is no big difference in the SNR in the case of 1700 nm. For the wavelength suggested to probe the epidermis layer, i.e., 1400, 1450, and 1500 nm, the SNR level is almost the same for all SDS less than 2 mm as shown in Fig. 6(b). For a longer SDS, the SNR level drops below 20 dB for SDS values larger than 6 mm for all the wavelengths. Though the SNR looks a little bit better for the 1400 nm, the epidermis sensitivity is better at 1450 nm than at 1400 nm. According to the dermis sensitivity presented in Fig. 4(a), the SDS should be 2 mm or larger in order to minimize its effect. Furthermore, considering the epidermis sensitivity presented in Fig. 4(b), the separation should be as small as possible to maximize the probed signal from the short channel. Therefore, a 2 mm separation at a wavelength of 1450 nm represents a potential choice for the short channel.

Based on the previous calculations and conclusions about the wavelengths and the SDSs, an example of the proposed dual channels final setup is presented in Fig. 7. In this example, the wavelength 1450 nm with a 2 mm SDS is used for the short channel, which has an epidermis

sensitivity of 30%. A considerable part of the signal is confined in the epidermis layer as can be observed with some of it scatter also into the dermis layer. For the long channel, the wavelength 1750 nm with a 6 mm SDS is used, which has a dermis sensitivity of 40%. This is reflected in the fact that a large portion of the signal propagates through the dermis layer. Nevertheless, one can witness that part of the signal is propagating through the epidermis layer as well as the subcutaneous layer. Note that decreasing the SDS will increase the sensitivity as shown in Fig. 4(b). In the future, the superficial noise measured by the short SDS channel can be removed using different well-developed algorithms [30], [33]–[35].

4. Conclusion

In this study, we evaluated the sensitivity of the epidermis and dermis layers at a broad range of wavelengths from 1200 nm to 1900 nm. The aim was to find the optimal wavelength with the optimal source-detector separation in order to remove the interference signal from the epidermis layer represented by the short channel from the total signal coming from the long channel. This challenging task was evaluated through Monte Carlo Simulations to find out the sensitivity and the SNR at all wavelengths for all SDS. Hence, the trade-off among the three important factors, i.e., SD separation, the source wavelengths, and the SNR was the core goal of this study. Knowledge of optimal short and long channel separations and wavelengths will allow for the design of a non-invasive CGM device where the noise from the epidermis layer can be measured with high sensitivity and ultimately be removed or largely suppressed. Thus, non-invasive blood glucose CGM measurements will be enhanced. In the future, this approach can pave the way for more reliable and accurate glucose monitoring sensors.

References

[1] I. L. Jernelv, K. Milenko, S. S. Fuglerud, D. R. Hjelme, R. Ellingsen, and A. Aksnes, "A review of optical methods for continuous glucose monitoring," *Appl. Spectrosc. Rev.*, vol. 54, no. 7, pp. 543–572, 2019, doi: 10.1080/05704928.2018.1486324.

[2] M. Shokrekhodaei, and S. Quinones, "Review of non-invasive glucose sensing techniques: Optical, electrical and breath acetone," *Sensors*, vol. 20, no. 5, Mar. 2020, Paper. MDPI AG, doi: 10.3390/s20051251.

[3] D. Bruen, C. Delaney, L. Florea, and D. Diamond, "Glucose sensing for diabetes monitoring: Recent developments," *Sensors*, vol. 17, no. 8, Aug. 2017, Paper. MDPI AG, doi: 10.3390/s17081866.

[4] R. A. Vigersky, "Going beyond HbA1c to understand the benefits of advanced diabetes therapies," *J. Diabetes*, vol. 11, no. 1, pp. 23–31, Jan. 2019, doi: 10.1111/1753-0407.12846.

[5] J. Huang, Y. Zhang, and J. Wu, "Review of non-invasive continuous glucose monitoring based on impedance spectroscopy," *Sensors Actuators, A: Phys.*, vol. 311. B.V. Elsevier, Ed., Aug. 2020, Art. no. 112103, doi: 10.1016/j.sna.2020.112103.

[6] W. V. Gonzales, A. T. Mobashsher, and A. Abbosh, "The progress of glucose monitoring—A review of invasive to minimally and non-invasive techniques, devices and sensors," *Sensors*, vol. 19, no. 4, Feb. 2019, doi: 10.3390/s19040800.

[7] D. B. Keenan, J. J. Mastrototaro, G. Voskanyan, and G. M. Steil, "Delays in minimally invasive continuous glucose monitoring devices: A review of current technology," *J. Diabetes Sci. Technol.*, vol. 3, no. 5, pp. 1207–1214, 2009, doi: 10.1177/193229680900300528.

[8] C. Chen *et al.*, "Recent advances in electrochemical glucose biosensors: A review," *RSC Adv.*, vol. 3, no. 14, 2013, doi: 10.1039/c2ra22351a.

[9] J. Wang, "Electrochemical glucose biosensors," *Chem. Rev.*, vol. 108, no. 2, 2008, doi: 10.1021/cr068123a.

[10] S. K. Vashist, "Non-invasive glucose monitoring technology in diabetes management: A review," *Analytica Chimica Acta*, vol. 750, 2012, doi: 10.1016/j.aca.2012.03.043.

[11] T. Fei, W. Xiaohao, W. Dongsheng, and L. Junfeng, "Non-invasive glucose measurement by use of metabolic heat conformation method," *Sensors*, vol. 8, pp. 3335–3344, 2008, doi: 10.3390/s8053335.

[12] S. A. Siddiqui, Y. Zhang, J. Lloret, H. Song, and Z. Obradovic, "Pain-free blood glucose monitoring using wearable sensors: Recent advancements and future prospects," *IEEE Rev. Biomed. Eng.*, vol. 11, pp. 21–35, 2018, doi: 10.1109/RBME.2018.2822301.

[13] S. Delbeck, T. Vahlsing, S. Leonhardt, G. Steiner, and H. M. Heise, "Non-invasive monitoring of blood glucose using optical methods for skin spectroscopy—Opportunities and recent advances," *Anal. Bioanal. Chem.*, vol. 411, pp. 63–77, Jan. 2019, doi: 10.1007/s00216-018-1395-x.

[14] S. Haxha, and J. Jhoja, "Optical based noninvasive glucose monitoring sensor prototype," *IEEE Photon. J,* vol. 8, no. 6, Dec. 2016, Art. no. 6805911, doi: 10.1109/JPHOT.2016.2616491.

[15] S. Y. Huang, Y. Zhang, J. Lloret, H. Song, and Z. Obradovic, "Microstrip line-based glucose sensor for noninvasive continuous monitoring using the main field for sensing and multivariable crosschecking," *IEEE Sensors J.*, vol. 19, no. 2, pp. 535–547, Jan. 2019, doi: 10.1109/JSEN.2018.2877691.

[16] Y. Marcus *et al.*, "Improving blood glucose level predictability using machine learning," *Diabetes. Metab. Res. Rev.*, vol. 36, no. 8, Nov. 2020, doi: 10.1002/dmrr.3348.
[17] K. Scholten, and E. Meng, "A review of implantable biosensors for closed-loop glucose control and other drug delivery applications," *Int. J. Pharm.*, vol. 544, no. 2, pp. 319–334, Jun. 2018, doi: 10.1016/j.ijpharm.2018.02.022.
[18] C. M. Girardin, C. Huot, M. Gonthier, and E. Delvin, "Continuous glucose monitoring: A review of biochemical perspectives and clinical use in type 1 diabetes," *Clin. Biochem.*, vol. 42, no. 3. 2009, doi: 10.1016/j.clinbiochem.2008.09.112.
[19] J. Liu, L. Jiang, H. Liu, and X. Cai, "A bifunctional biosensor for subcutaneous glucose monitoring by reverse iontophoresis," *J. Electroanal. Chem.*, vol. 660, no. 1, 2011, doi: 10.1016/j.jelechem.2011.05.012.
[20] R. O. Potts, J. A. Tamada, and M. J. Tierney, "Glucose monitoring by reverse iontophoresis," *Diabetes. Metab. Res. Rev.*, vol. 18, no. SUPPL. 1, 2002, doi: 10.1002/dmrr.210.
[21] A. Caduff, E. Hirt, Y. Feldman, Z. Ali, and L. Heinemann, "First human experiments with a novel non-invasive, non-optical continuous glucose monitoring system," *Biosens. Bioelectron.*, vol. 19, no. 3, 2003, doi: 10.1016/S0956-5663(03)00196-9.
[22] I. M. E. Wentholt, J. B. L. Hoekstra, A. Zwart, and J. H. DeVries, "Pendra goes dutch: Lessons for the CE mark in europe," *Diabetologia*, vol. 48, no. 6, 2005, doi: 10.1007/s00125-005-1754-y.
[23] E. Tsalikian, "Accuracy of the glucowatch G2 biographer and the continuous glucose monitoring system during hypoglycemia: Experience of the diabetes research in children network," *Diabetes Care*, vol. 27, no. 3, 2004, doi: 10.2337/diacare.27.3.722.
[24] M. R. Robinson *et al.*, "Noninvasive glucose monitoring in diabetic patients: A preliminary evaluation," *Clin. Chem.*, vol. 38, no. 9, 1992, doi: 10.1093/clinchem/38.9.1618.
[25] U. A. Muller, B. Mertes, C. Fischbacher, K. U. Jageman, and K. Danzer, "Non-invasive blood glucose monitoring by means of near infrared spectroscopy: Methods for improving the reliability of the calibration models," *Int. J. Artif. Organs*, vol. 20, no. 5, 1997, doi: 10.1177/039139889702000509.
[26] J. P. Bantle, and W. Thomas, "Glucose measurement in patients with diabetes mellitus with dermal interstitial fluid," *J. Lab. Clin. Med.*, vol. 130, no. 4, pp. 436–441, 1997, doi: 10.1016/S0022-2143(97)90044-5.
[27] S. N. Thennadil, J. L. Rennert, B. J. Wenzel, K. H. Hazen, T. L. Ruchti, and M. B. Block, "Comparison of glucose concentration in interstitial fluid, and capillary and venous blood during rapid changes in blood glucose levels," *Diabetes Technol. Ther.*, vol. 3, no. 3, pp. 357–365, 2001, doi: 10.1089/152091501526071132.
[28] K. Maruo *et al.*, "Noninvasive blood glucose assay using a newly developed near-infrared system," *IEEE J. Sel. Topics Quantum Electron.*, vol. 9, no. 2, pp. 322–330, Mar. 2003, doi: 10.1109/JSTQE.2003.811283.
[29] R. B. Saager, and A. J. Berger, "Direct characterization and removal of interfering absorption trends in two-layer turbid media," *J. Opt. Soc. Amer A*, vol. 22, no. 9, 2005, doi: 10.1364/josaa.22.001874.
[30] L. Gagnon, M. A. Yücel, D. A. Boas, and R. J. Cooper, "Further improvement in reducing superficial contamination in NIRS using double short separation measurements," *Neuroimage*, vol. 85, pp. 127–135, 2014.
[31] M. Althobaiti, and I. Al-Naib, "Recent developments in instrumentation of functional near-infrared spectroscopy systems," *Appl. Sci.*, vol. 10, no. 18. 2020, doi: 10.3390/APP10186522.
[32] S. Brigadoi, and R. J. Cooper, "How short is short? Optimum source–detector distance for short-separation channels in functional near-infrared spectroscopy," *Neurophotonics*, vol. 2, no. 2, 2015, doi: 10.1117/1.nph.2.2.025005.
[33] L. Gagnon, K. Perdue, D. N. Greve, D. Goldenholz, G. Kaskhedikar, and D. A. Boas, "Improved recovery of the hemodynamic response in diffuse optical imaging using short optode separations and state-space modeling," *Neuroimage*, vol. 56, no. 3, 2011, doi: 10.1016/j.neuroimage.2011.03.001.
[34] L. Gagnon, R. J. Cooper, M. A. Yücel, K. L. Perdue, D. N. Greve, and D. A. Boas, "Short separation channel location impacts the performance of short channel regression in NIRS," *Neuroimage*, vol. 59, no. 3, 2012, doi: 10.1016/j.neuroimage.2011.08.095.
[35] R. B. Saager, N. L. Telleri, and A. J. Berger, "Two-detector corrected near infrared spectroscopy (C-NIRS) detects hemodynamic activation responses more robustly than single-detector NIRS," *Neuroimage*, vol. 55, no. 4, 2011, doi: 10.1016/j.neuroimage.2011.01.043.
[36] X. Zhou, G. Sobczak, C. M. McKay, and R. Y. Litovsky, "Comparing fNIRS signal qualities between approaches with and without short channels," *PloS One*, vol. 15, no. 12, Dec. 2020, Art. no. e0244186.
[37] G. Han, X. Yu, D. Xia, R. Liu, J. Liu, and K. Xu, "Preliminary clinical validation of a differential correction method for improving measurement accuracy in noninvasive measurement of blood glucose using near-infrared spectroscopy," *Appl. Spectrosc.*, vol. 71, no. 9, pp. 2177–2186, 2017, doi: 10.1177/0003702816685335.
[38] J. Liu, C. Zhu, J. Jiang, and K. Xu, "Scattering-independent glucose absorption measurement using a spectrally resolved reflectance setup with specialized variable source-detector separations," *Biomed. Opt. Exp.*, vol. 9, no. 12, Dec. 2018, doi: 10.1364/boe.9.005903.
[39] J. Liu, T. Han, J. Jiang, and K. Xu, "Specialized source-detector separations in near-infrared reflectance spectroscopy platform enable effective separation of diffusion and absorption for glucose sensing," *Biomed. Opt. Exp.*, vol. 10, no. 9, Sep. 2019, doi: 10.1364/boe.10.004839.
[40] Q. Fang, and D. A. Boas, "Monte carlo simulation of photon migration in 3D turbid media accelerated by graphics processing units," *Opt. Exp.*, vol. 17, no. 22, pp. 20178–20190, 2009.
[41] S. Yan, and Q. Fang, "Hybrid mesh and voxel based Monte Carlo algorithm for accurate and efficient photon transport modeling in complex bio-tissues," *Biomed. Opt. Exp.*, vol. 11, no. 11, 2020, doi: 10.1364/boe.409468.
[42] T. L. Troy, and S. N. Thennadil, "Optical properties of human skin in the near infrared wavelength range of 1000 to 2200 nm," *J. Biomed. Opt.*, vol. 6, no. 2, pp. 167–176, 2001, doi: 10.1117/1.1344191.
[43] C. R. Simpson, M. Kohl, M. Essenpreis, and M. Cope, "Near-infrared optical properties of ex vivo human skin and subcutaneous tissues measured using the Monte Carlo inversion technique," *Phys. Med. Biol.*, vol. 43, no. 9, 1998, Art. no. 2465, doi: 10.1088/0031-9155/43/9/003.
[44] Y. Yuan, L. Yu, Z. Doğan, and Q. Fang, "Graphics processing units-accelerated adaptive nonlocal means filter for denoising three-dimensional Monte Carlo photon transport simulations," *J. Biomed. Opt.*, vol. 23, no. 12, 2018, doi: 10.1117/1.jbo.23.12.121618.